Supporting Information

Achieving high thermoelectric performance through constructing coherent interfaces and building interface potential barriers in n-type $Bi_2Te_3/Bi_2Te_{2.7}Se_{0.3}$ nanocomposites

Bushra Jabar [a,b], Xiaoying Qin,[a,], Di Li [a] , Jian Zhang [a] , Adil Mansoor [a] , Hongxing Xin [a] , Chunjun Song [a] , Lu.Lu. Huang [a,b]*

[a] Key laboratory of Material Physics, Institute of Solid State Physics, Chinese Academy of Sciences, Hefei 230031, China.
E-mail: xyqin@issp.ac.cn.
[b] University of Science and Technology of China, Hefei 230026, China.

*Corresponding author
Xiaoying Qin,
Key laboratory of Material Physics, Institute of Solid State Physics, Chinese Academy of Sciences, Hefei 230031, China.
E-mail: xyqin@issp.ac.cn.

1. The analysis of preferred orientation

The (001) preferred orientation possible in all the composites specimens $\beta Bi_2Te_3/Bi_2Te_{2.7}Se_{0.3}$ (β=0, 0.1 to 0.3, 0.5 and 0.8 vol.%) was analyzed. The orientation factor F can be determined as following [1]

$$F = \frac{p - p_o}{p - p_o}; p = \frac{I(00l)}{\sum I(hkl)}, p_o = \frac{I_o(00l)}{\sum I_o(hkl)} \quad \text{(S-1)}$$

where p and p_o represents the ratio integrated intensities of all *(00l)* plane to the summation of all *(hkl)* plane intensities for composite and reference specimen, respectively. The calculated F values are 0.10, 0.16, 0.11, 0.14 and 0.05 for β=0, 0.1, 0.3, 0.5 and 0.8 vol.%, respectively, as

shown in table S1. The obtained result indicates that there is more or less preferred (001) orientation for every specimen.

However, one notices that among composite specimens the orientation factor F (0.14) for the specimen with β=0.5 vol.% is apparently larger than that (F=0.11) for the specimen with β=0.3 vol.%, which should impact their electrical transport properties (as discussed in main text).

Table S1. A list of (001) preferred orientation factor F for all the composite specimens $\beta Bi_2Te_3/Bi_2Te_{2.7}Se_{0.3}$ (β=0, 0.1 to 0.3, 0.5 and 0.8 vol.%)

β (vol.%)	0	0.1	0.3	0.5	0.8
F	0.10	0.16	0.11	0.14	0.05

2. Rietveld refinement analysis

Rietveld refinement analyses for all specimens $\beta Bi_2Te_3/Bi_2Te_{2.7}Se_{0.3}$ (β=0. 0.1, 0.3, 0.5 and 0.8 vol. %) are performed, as shown in Fig. S1(a)-(e). The results indicate that the contents of secondary phase Bi_2Te_3 in composite specimens are in good agreement with the incorporated content (β) in $\beta Bi_2Te_3/Bi_2Te_{2.7}Se_{0.3}$, as given in table S2.

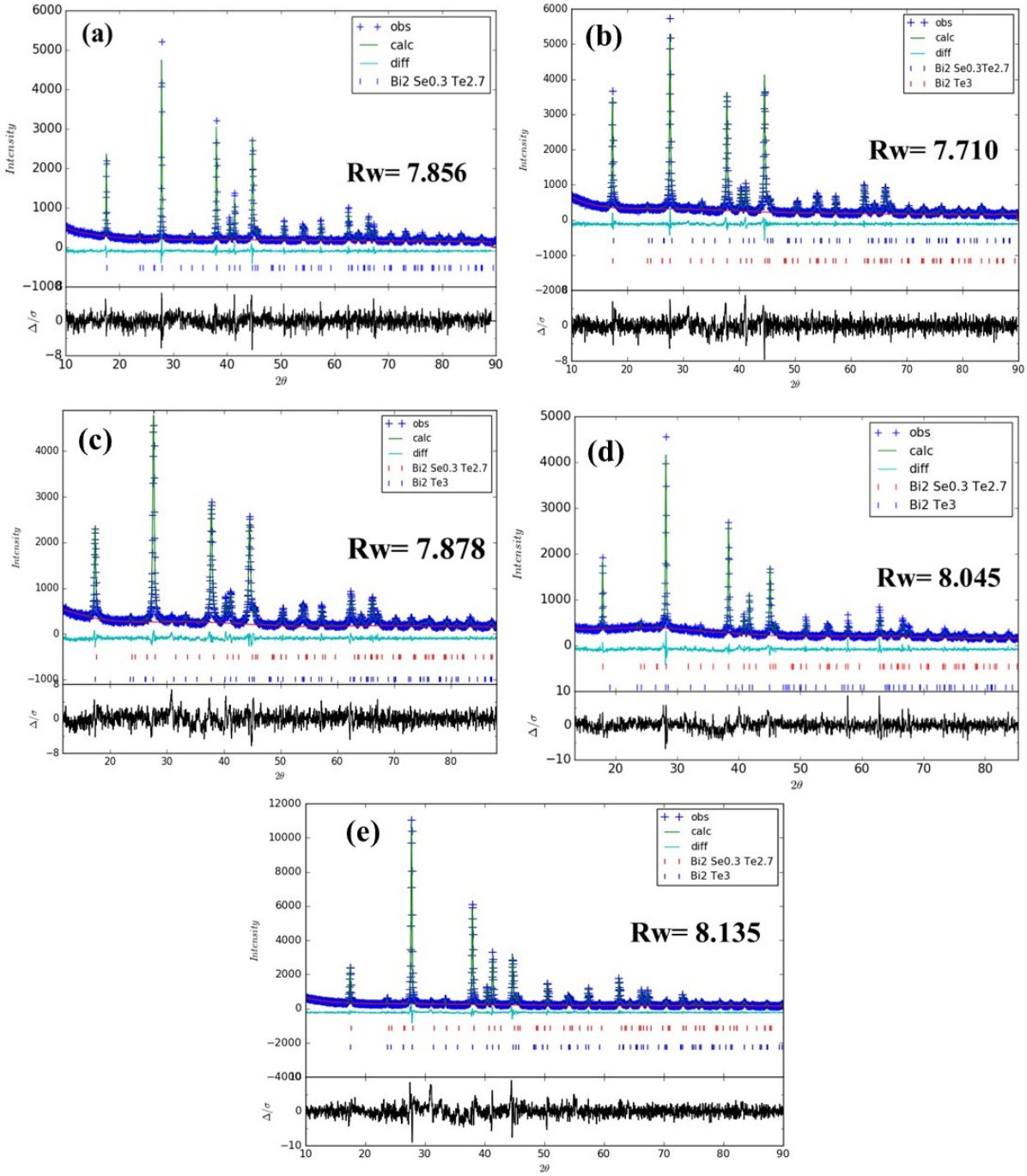

Figure S1. (a) Rietveld refinement analysis for $\beta Bi_2Te_3/Bi_2Te_{2.7}Se_{0.3}$ (a) with β=0, (b) β=0.1 (c) β=0.3 and (d) β=0.5 and (e) β=0.8 vol.% where obs, calc, and diff represents observed, calculated and residual differences between the two curves.

Table S2. Rietveld refinement parameters for $\beta Bi_2Te_3/Bi_2Te_{2.7}Se_{0.3}$ (β=0, 0.1, 0.3, 0.5 and 0.8 vol.%)

β vol.%	R_{exp} (%)	R_w (%)	Bi_2Te_3 (vol.%)	GOF
0	6.04	7.856	0	1.30
0.1	5.468	7.710	0.08	1.41
0.3	5.396	7.878	0.20	1.46
0.5	5.5868	8.045	0.44	1.44
0.8	4.990	8.135	1.00	1.63

3. Microstructure characterizations by using FE-SEM and EDS.

The microstructures of BTS, BT inclusions and composite bulk specimens $\beta Bi_2Te_3/Bi_2Te_{2.7}Se_{0.3}$ were further investigated by using field emission scanning electron microscopy (FE-SEM) and energy dispersive X-ray spectroscopy (EDX). FE-SEM observations show that the particles of BTS matrix powders have the dimensions of micrometers (Fig. S2(a)); while most of Bi_2Te_3 particles have sizes of ~50 nm (Fig. S2(b) and Fig. S3). Appropriately, on the fracture surface of the composite specimens (β=0.5vol%, for instance) (Fig. S2(c)) one can find out some nanoparticles with size of 50-100nm, corresponding to which there is a shortage of element Se, as shown by element mapping of EDX (Fig. S2(e)). Hence these particles on the fracture surface can be ascribed to Bi_2Te_3 inclusions.

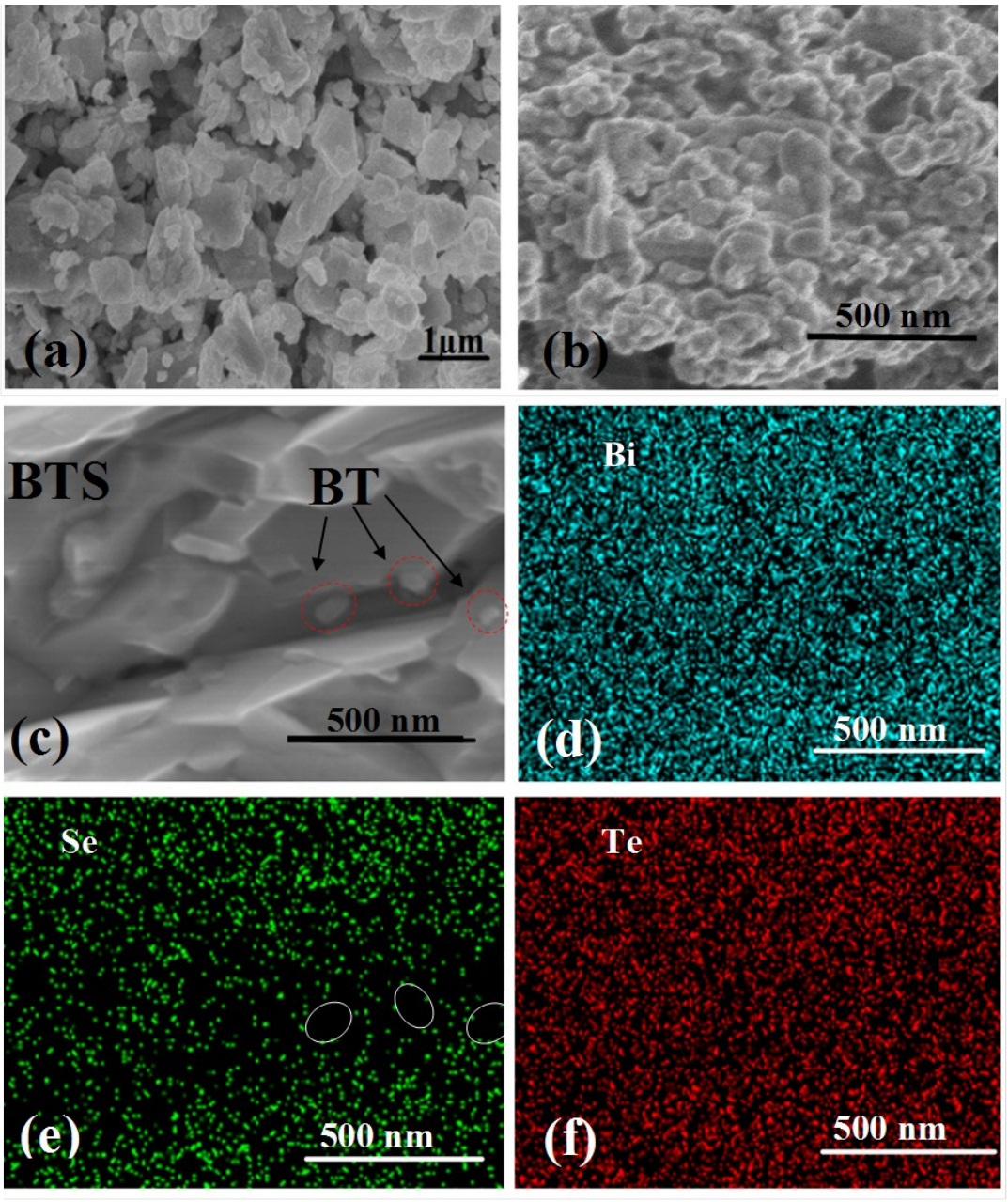

Figure S2. (a) FE-SEM micrographs of powders of $Bi_2Te_{2.7}Se_{0.3}$ and (b) Bi_2Te_3 nanoparticles (c) EDX analysis for composite specimen f =0.5vol% at 500nm; (d) a EDX mapping for element Bi (e) for Se and (f) for Te element in selected area for specimen f =0.5 vol%.

4. Statistical analysis result of size distribution of Bi_2Te_3 nanoparticles

We statistically analyzed the size distribution of Bi_2Te_3 nanoparticles, based on the FE-SEM observations (as shown in Fig. S2(b)). Fig. S3 gives the results, which indicates that most of Bi_2Te_3 particles have sizes of ~50 nm.

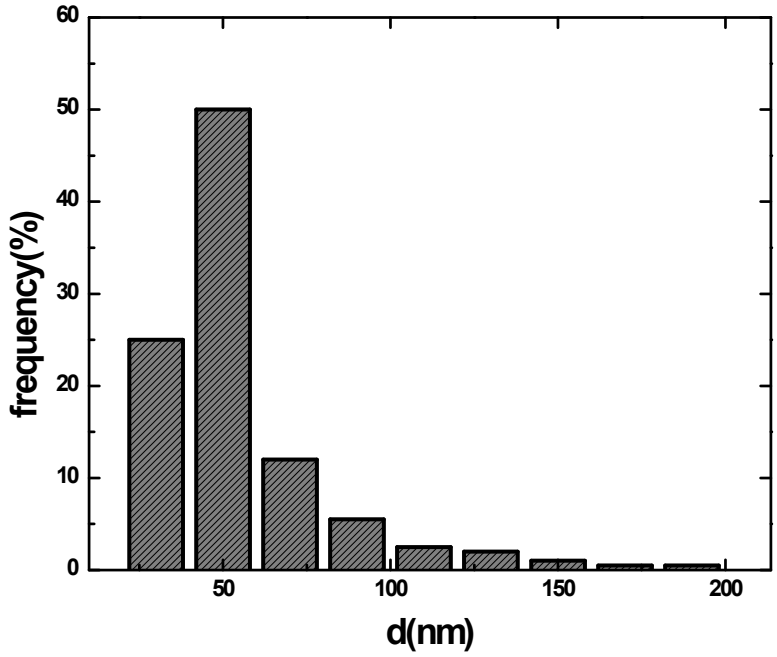

Figure S3. Size distribution of Bi_2Te_3 nanoparticles.

5. The change of electronic concentration, mobility and resistivity (at 300 K) of the specimens with different BT content *β*

The electrical resistivity (ρ) is determined by carrier concentration (*n*) and mobility (μ) and there is a relation ρ = 1/neμ. Hence, the relative change of the resistivity $\frac{\Delta\rho}{\rho}$ is related to relative change of carrier concentration Δn/n and mobility Δμ/μ by the relation $\frac{\Delta\rho}{\rho} = \frac{\Delta n}{n} + \frac{\Delta\mu}{\mu}$ -(). In the

composite specimens $\beta Bi_2Te_3/Bi_2Te_{2.7}Se_{0.3}$, the variations of the resistivity are directly associated with change of both carrier concentration and mobility. Table S3-1 shows electronic concentration (n) and mobility (μ) for all $\beta Bi_2Te_3/Bi_2Te_{2.7}Se_{0.3}$ specimens. The relative changes of concentration, mobility and the resistivity for specimens with different β are given in table S3-2.

Table S3-1 The carrier concentration (n) and mobility (μ) (at 300K) for specimen $\beta Bi_2Te_3/Bi_2Te_{2.7}Se_{0.3}$ (β=0, 0.1, 0.3, 0.5 and 0.8 vol.%)

β(vol.%)	0	0.1	0.3	0.5	0.8
n ($\times 10^{19} cm^{-3}$)	6.43	6.96	7.34	7.94	8.74
μ ($cm^2V^{-1}s^{-1}$)	122.5	128.2	104.9	108.8	83.4

Table S3-2 Relative changes of n, μ and ρ (at 300K) for $\beta Bi_2Te_3/Bi_2Te_{2.7}Se_{0.3}$ specimens with different β

β_j-β_i (vol.%)	0.1-0.0	0.3- 0.1	0.5- 0.3	0.8-0.5
$\Delta n/n$ (%)	8.24	5.58	8.18	10.00
$\Delta\mu/\mu$ (%)	4.68	-18.22	3.73	-23.29
$\Delta\rho/\rho$ (%)	-12.92	12.64	-11.91	13.29

Annotation: β_j-β_i stands for relative changes of the properties (Δn/n, $\Delta\mu/\mu$ and $\Delta\rho/\rho$) of the composite speciem with β_j (e.g. β_j =0.3 vol.%) as compared to those of the specimen with β_i (e.g. β_i =0.1 vol.%), which simply written as: 0.3- 0.1 (vol.%), as shwon in third column.

6. Dependence of PF on carrier concentration

Fig. S4 shows the dependence of power factor PF on carrier concentration n for matrix BTS (solid line) (at 300 K). One can see clearly that PF for the composite specimens with β =0.1 and 0.5 vol.% (red hexagonal and blue square, respectively) enhances substantially as compared to that of BTS matrix.

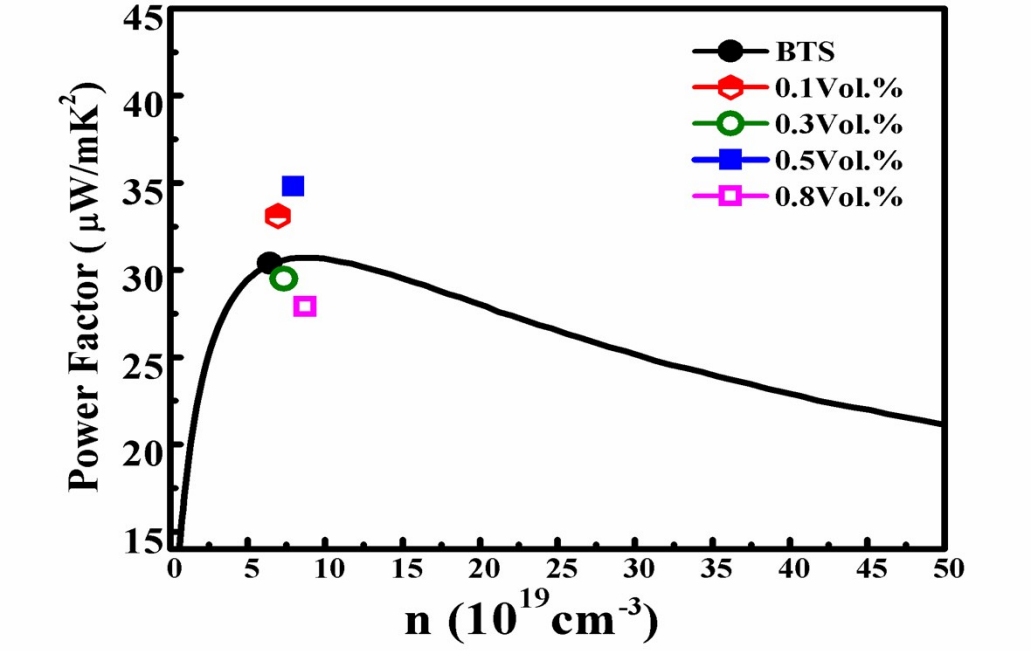

Figure S4. The dependence of power factor on carrier concentration for matrix BTS (at 300 K), where the values of PF for composite specimens $\beta Bi_2Te_3/Bi_2Te_{2.7}Se_{0.3}$ (β=0, 0.1 to 0.3, 0.5 and 0.8 vol. %) are also illustrated.

7. Measurement of density

We have measured densities for all of the samples by using Archimedes method, and the results indicated that the relative densities d_r of all of our samples are very high, reaching 98-99% , as shwon in the table S3.

Table S4. Densities d and relative densities d_r for all the composite specimens $\beta Bi_2Te_3/Bi_2Te_{2.7}Se_{0.3}$ (β= 0, 0.1, 0.3, 0.5 and 0.8 vol.%)

β vol.%	d	d_r
0	7.87	99.4
0.1	7.8	98.6
0.3	7.84	99.1
0.5	7.75	97.9
0.8	7.74	97.8

where d_r is relative density, defined as $d_r=d/d_o$, here d is the measured density and d_o (7.91 of g cm^{-3}) is the theoratical density of $Bi_2Te_{2.7}Se_{0.3}$. For composite specimens $\beta Bi_2Te_3/Bi_2Te_{2.7}Se_{0.3}$, the theoretical density is modified as: $d_o= [1-\beta]\ d_1 + \beta d_2$, where $d_1=d_o$ for BTS matrix and d_2 (7.86 g cm^{-3}) is the theoratical density of Bi_2Te_3.

8. Measurement of specific heat

The specific heat for BTS matrix and composite specimens was determined by DSC, which shows that the obtained C_{pm} for BTS almost equals to Dulong-Petit law, as given in the Fig. S5. The specific heat C_{pc} for composite specimens is actually same as that of BTS (within experimental error) due to both BT having similar specific heat to BTS and very small contents of BT in BTS matrix.

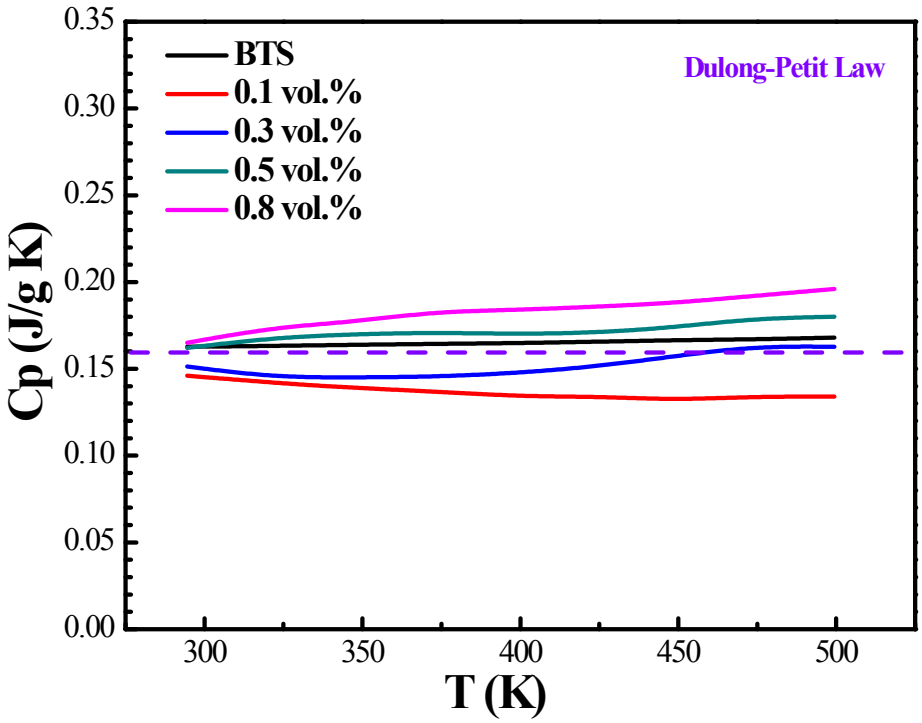

Figure S5. (a) Temperature dependent specific heat capacity C_{pm} for $Bi_2Te_{2.7}Se_{0.3}$ and C_{pc} for βBT/BTS with β=0 , 0.1, 0.3, 0.5 and 0.8 vol.%.

9. Repeatability and thermal stability (at T≤ 525K) of the thermoelectric properties for our BTS composite specimen (incorporated with 0.5 vol.% BT)

We conducted experiments to show repeatability and thermal stability for BTS based composites with BT nanoinclusions (β=0.5 vol. %, for instance), as shown below.

(1) Repeatability

The electrical resistivity ρ (a), thermopower S (b) and total thermal conductivity κ (c) were measured for three specimens (specimens 1#, 2# and 3#) (as given in Fig. R3 below), and the results indicated that repeatability of the specimen properties is good with standard deviation for ρ, S and κ is ±3%-±4%, ±1%-±2% and ±4%-±5% at 300K and 525K, respectively. According to error propagation theory:

Since $Z = \frac{S^2}{\rho \bullet \kappa}$ (S-2)

then,

$$\Delta Z = \left|\frac{2S^2}{\rho\ \kappa\ S}\frac{\Delta S}{}\right| + \left|\left(-\frac{S^2}{\kappa}\ \frac{1}{\rho}\frac{\Delta\rho}{\rho}\right)\right| + \left|\left(-\frac{S^2}{\rho}\ \frac{1}{\kappa}\frac{\Delta\kappa}{\kappa}\right)\right|$$

$$\frac{\Delta ZT}{ZT} = \frac{\Delta Z}{Z} = \frac{\frac{\Delta Z}{S^2}}{\rho\ \kappa}$$

$$= \left|2\frac{\Delta S}{S}\right| + \left|-\frac{\Delta\rho}{\rho}\right| + \left|-\frac{\Delta\kappa}{\kappa}\right| \quad \text{(S-3)}$$

As we replace $\frac{\Delta\rho}{\rho}$, $\frac{\Delta S}{S}$ and $\frac{\Delta\kappa}{\kappa}$ with the values of standard deviation for ρ, S and κ in formula (S-3), we obtained accuracy for the measurements of ZT is:

$$\frac{\Delta ZT}{ZT} = \pm(|2\frac{\Delta S}{S}| + |-\frac{\Delta \rho}{\rho}| + |-\frac{\Delta \kappa}{\kappa}|)$$

$$= \pm(|2\times 2\%| + |4\%| + |5\%|) = \pm 13\ \%\ (\text{at } 525\ \text{K})$$

Or $= \pm(|2\times 1\%| + |3\%| + |4\%|) = \pm 9\ \%\ (\text{at } 300\ \text{K})$

Now, we calculated accuracy for the measurements of ZT at all the temperatures, which is shown as error bars in Fig. 7(d).

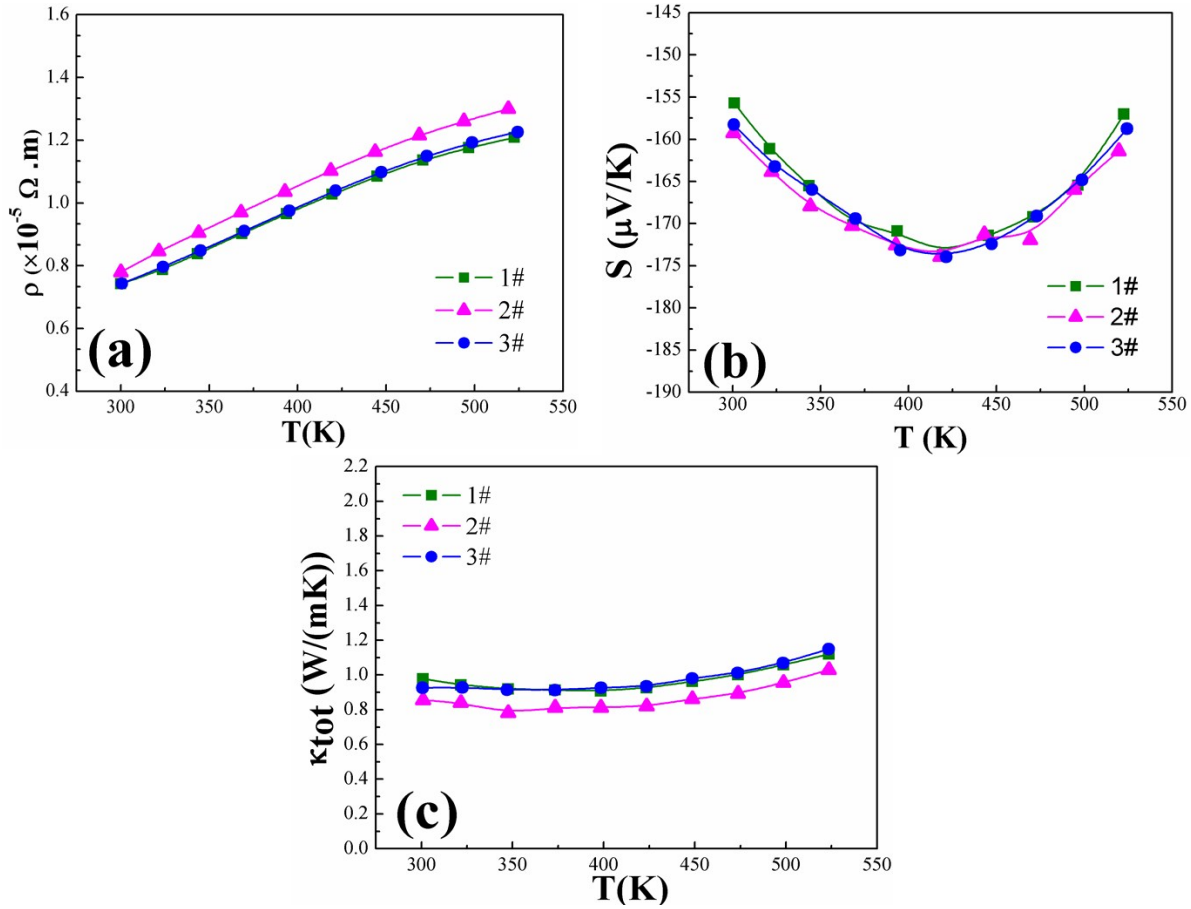

Figure S6. Repeatability measurements for three βBT/BTS specimens with β= 0.5 vol.% (a) Temperature dependent electrical resistivity (b) thermopower and (c) total thermal conductivity.

(2) Thermal stability at T≤ 525K

The heating-cooling data of electrical resistivity (a), thermopower (b) and total thermal conductivity (c), as shown in Fig. S7 below, can be repeated completely (with experimental errors) for the first, second and third heat-cooling cycle, indicate that our BTS based composites incorporated with BT nanoinclusions have good thermal stability at temperature range T=300K-525K.

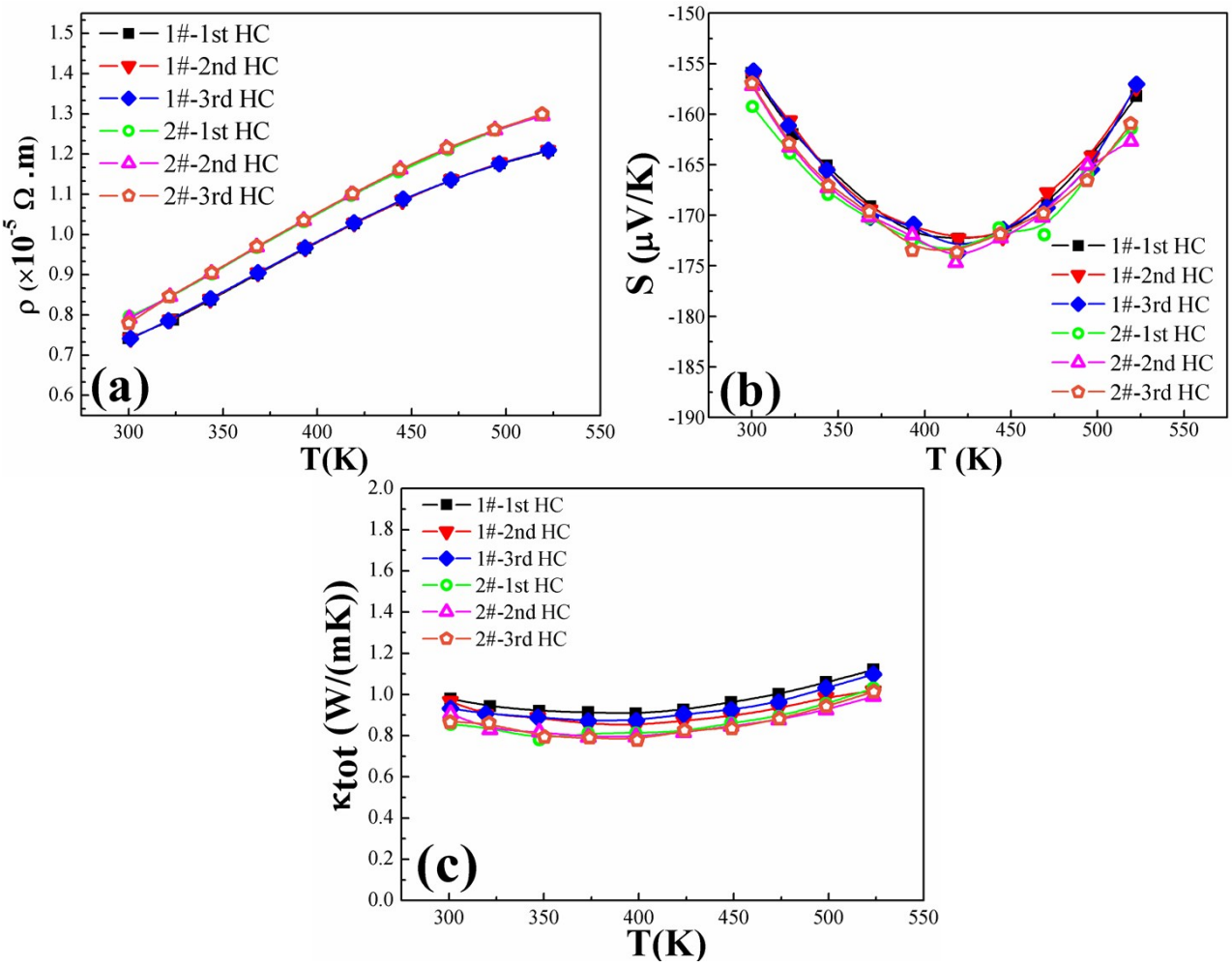

Figure S7. Thermal stability measurements (at T≤ 525K) for βBT/BTS with β= 0.5 vol.% (a) Temperature dependent electrical resistivity (b) thermopower and (c) total thermal conductivity, wherein the symbol 1st HC, 2nd HC and 3rd HC stand for the first, second and third heating-cooling measurements; 1# and 2# represent specimen 1 and specimen 2.

10. Comparison of *ZT* and thermoelectric conversion efficiency η in low temperature range for our BTS composite specimen (incorporated with 0.5 vol.% BT) obtained in

present work and other typical n-type TE materials reporting high thermoelectric performance.

Fig. S8 and **S9** show temperature dependent figure of merit *ZT* value comparison for low-temperature BTS system (present work) and other typical medium-temperature n-type thermoelectric material systems [2-9]. Moreover, both thermoelectric conversion efficiency η at T<300 °C and ZT_{max} of present optimized BTS system are more competitive than most of the state-of-the-art medium-temperature n-type TE materials, for room temperature applications (as shown in **Fig. S8** and **S9**).

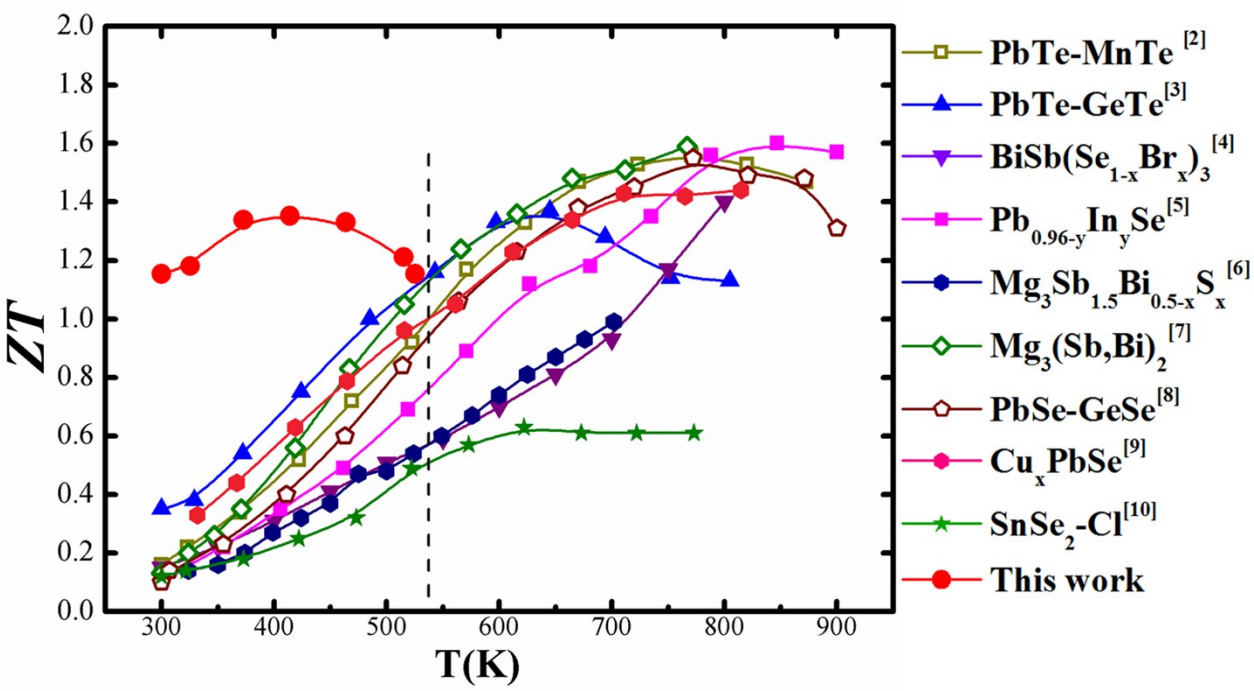

Figure S8. Temperature dependence of figure of merit *ZT* of our BTS based composite specimen (incorporated with 0.5 vol.% BT) and other typical n-type thermoelectric material systems reporting high thermoelectric performance. Therein one can see that the *ZT* values at T<530 K for our BTS system (present work) is much larger than the *ZT* values in corresponding temperature range for several typical n-type thermoelectric material systems reporting high thermoelectric performance[2-9].

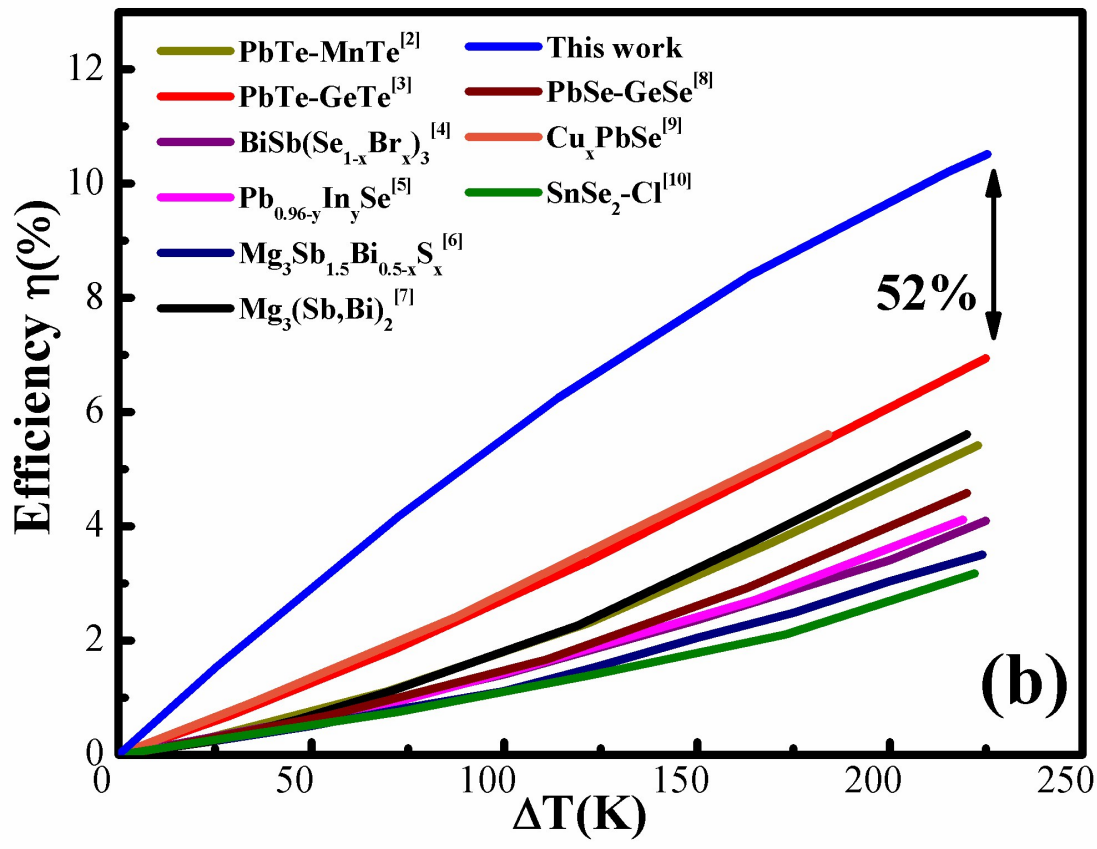

Figure S7. Comparison of thermoelectric conversion efficiency η in low temperature range for our BTS composite specimen (incorporated with 0.5 vol.% BT) obtained in present work and other typical n-type TE materials reporting high thermoelectric performance. One can see that conversion efficiency η of our BTS composite specimen is much (at least 52% at T=525 K) larger than that of other high reported *ZT* values n-type thermoelectric material systems[2-9].

References

[1] Y. Pan, J.-F. Li, Npg Asia Materials, 8 (2016) e275.

[2] L.-D. Zhao, Y. Xiao, H. Wu, J. Cui, D. Wang, L. Fu, Y. Zhang, Y. Chen, J. He, S.J. Pennycook, Energy & Environmental Science, (2018).

[3] Z.Z. Luo, X. Zhang, X. Hua, G. Tan, T.P. Bailey, J. Xu, C. Uher, C. Wolverton, V.P. Dravid, Q. Yan, Advanced Functional Materials, (2018) 1801617.

[4] X. Liu, D. Wang, H. Wu, J. Wang, Y. Zhang, G. Wang, S.J. Pennycook, L.-D. Zhao, Advanced Functional Materials, 0 1806558.
[5] M. Hong, Z.-G. Chen, S. Matsumura, J. Zou, Nano Energy, 50 (2018) 785-793.
[6] J. Zhang, L. Song, K.A. Borup, M.R.V. Jørgensen, B.B. Iversen, Advanced Energy Materials, (2018) 1702776.
[7] J. Shuai, B. Ge, J. Mao, S. Song, Y. Wang, Z. Ren, Journal of the American Chemical Society, 140 (2018) 1910-1915.
[8] L. You, Y. Liu, X. Li, P. Nan, B. Ge, Y. Jiang, P. Luo, S. Pan, Y. Pei, W. Zhang, Energy & Environmental Science, (2018).
[9] Y. Luo, Y. Zheng, Z. Luo, S. Hao, C. Du, Q. Liang, Z. Li, K.A. Khor, K. Hippalgaonkar, J. Xu, Advanced Energy Materials, 8 (2018) 1702167.